Sensors and Materials, Vol. 36, No. 12 (2024) 5341–5352
MYU Tokyo

S & M 3871

Intelligent Muscle Assessment Using a Sound Injection Sensor and Generative Adversarial Optimization

Yenming J. Chen,[1,2†] Kao-Shing Hwang,[2,3†] Jinn-Tsong Tsai,[2,4]
Chien-Ming Wu,[5*] and Wen-Hsien Ho[2,6,7**]

[1]Department of Information Management, National Kaohsiung University of Science and Technology, Kaohsiung 824, Taiwan
[2]Department of Healthcare Administration and Medical Informatics, Kaohsiung Medical University, Kaohsiung 807, Taiwan
[3]Department of Electrical Engineering, National Sun Yat-Sen University, Kaohsiung 804, Taiwan
[4]Department of Computer Science and Artificial Intelligence, National Pingtung University, Pingtung 900, Taiwan
[5]Department of Physical Medicine and Rehabilitation, Yuan's General Hospital, Kaohsiung 802, Taiwan
[6]Department of Medical Research, Kaohsiung Medical University Hospital, Kaohsiung 807, Taiwan
[7]College of Professional Studies, National Pingtung University of Science and Technology, Pingtung 912, Taiwan

(Received May 26, 2024; accepted October 15, 2024)

Keywords: reactive phonomyography, strength assessment, sound injection resonance myophonogram, machine learning, digital twin, generative adversarial network

In this study, we developed a low-cost, portable, and electrode-free intelligent device for the nondestructive evaluation of the muscle cross section of rehabilitation patients or elderly individuals. Currently, muscle quality is mostly explored by personal feelings. There is no convenient instrument that can quantify daily training progress on the local muscle level. Such a device can significantly encourage and motivate the elderly and rehabilitation patients to participate in a training program. Our sound injection resonant myophonogram can overcome the many challenges of existing muscle measurement devices. We actively injected a sound wave spectrum into the deep layers of the muscle to form a wavefront field. The reflected sound spectrum was then formed through the interaction of minute shear elasticity generated by the muscle tissue on the resonant point between the expansion and contraction of tissues. We employed an optimization algorithm on the generative adversarial network to learn the parameters of the muscle model and translated the responses into a performance index. To achieve such real-time predictive feedback, we implemented a sound excitation device and a cloud computing service to develop the algorithm with high performance at a low cost. Our device has been proven accurate and can perform measurements in real time. The device's assessment achieved an accuracy of more than 90% in 0.5 s.

[†]Equal contributors
[*]Corresponding author: e-mail: chienming.pmr@gmail.com
[**]Corresponding author: e-mail: whho@kmu.edu.tw
https://doi.org/10.18494/SAM5338

1. Introduction

Although national sports teams use precision instruments during their training, the personal training of ordinary people may not do so. Because an average person may not have the instrument to observe tissue and cellular changes during training, the training program involving load increase should be conservative to avoid injury. However, the extent of conservativeness would vary from person to person, time to time, and place to place. Additionally, the consequence of overloaded shock cannot be easily observed. The interaction between recovery compensation and psychological hormones could have inflicted damage before the trainer noticed it. Therefore, it is often too late and irreparable when a symptom emerges. Existing approaches, such as electromyography (EMG), myophonogram, or ultrasound, are expensive and impractical for daily training use.

In this study, we aimed to implement a sound-based device that is cheap and portable. After absorption and conduction, reflection sounds traverse to the deep layers of the muscle and are affected by muscle elasticity. Therefore, the received sounds contain rich muscle information and can be expressed as an easy-to-use muscle strength index by an artificial intelligence method. In this way, a lab-grade training program can be achieved with a low-cost personal device, and the asymptotic intensity of overload resistance training can be tailor-made according to the marginal situation of the muscle, and, therefore, the training objectives can be precisely achieved without injury.

Previous muscle measurement devices have disadvantages. Mechanomyography (MMG) or surface EMG is not easy for ordinary people to perform, and ultrasonic devices are even expensive and professional. The analysis methods hamper classical approaches; therefore, convenient sensing methods are desired to make the analysis easy. Our sound injection resonance myophonogram (SIRM) needs only a pair of ordinary audio devices to measure the deep properties of the muscle. The response of sound injection is analyzed to isolate the interference from multiple reflection paths. Our sparse ensemble assimilation (SEA) technology can recover the interference without overfitting.

Although the principle of sound field analysis is well developed, it is still limited by computation methods and cross-discipline capabilities, so it has not been paid sufficient attention in the health community. This study is timely in reopening this aspect of the study based on the development of artificial intelligence, leading to the study of an effective muscle measurement device. This study's real-time predictive muscle index can be used to achieve high-performance training using a low-cost device.

Despite many related studies on automatic muscle assessment, most focus on EMG, myosphonogram, or ultrasound, which may not be suitable for home use. Our innovative sound method focuses on audible sounds, which is different from existing methods.

Ultrasound imaging is probably the most popular and de facto evaluation method for determining muscle atrophy.[1–3] However, the relatively expensive cost and the requirement of human expert assistance hinder its application to personal usage for assessment in daily activities. EMG can also detect muscle atrophy in a clinical environment.[4] The complex form of neuromuscular signals also prevents the accuracy of automatic diagnosis. MMG sensors have been discussed extensively, but few of them can be used for long-term monitoring.[5]

The acoustical assessment of muscle function in long-term and daily monitoring is reported with good reproducibility.[6] Acoustic emission has been associated with muscular tissue deformation.[7] The mechanical properties of the muscle are complex and show rich anisotropy[8] and, therefore, cannot be directly derived from the simple pitches and amplitudes of reflection sound.[9,10] In both human and animal experiments, the representative patterns of sound reflection through a particular part of the muscle are recorded.[10,11] The shear modulus of the human muscle can be measured by ultrasound shear wave elastography,[12] which has been proven effective in assessing the muscle-tendon unit through mechanical responses.[13] Ultrasound shear wave elastography can also be used to evaluate muscle fatigue on the basis of static shear modulus.[3,14]

Conventionally, trainers and coaches can only rely on a few muscle grading systems to categorize the levels of recovery conditions. Manual muscle tests by the Medical Research Council (MRC) are commonly adopted for instrument-free assessment.[15] A modified scale was also proposed to test muscle strength for radial palsy patients.[16] The Oxford grading scale was used for pelvic floor strength for nulliparous sports students.[17] Portable sensor devices have also been developed for dysphagia.[18,19] A commercially initiated system, ESTi® score [efficiency/coordination (E-score), spatial summation (S-score), and temporal summation (T-score)], is used for muscle strength assessment.[9]

Sonomyography usually emits ultrasound and estimates the tissue composition by measuring the sound traverse time. Acoustic myography (AMG) usually estimates the characteristics of the tissue by analyzing the received sound spectrum. Some AMGs passively take the sounds produced by muscle contraction, whereas others receive the reflected sounds from an active sound source.[5] The passive AMG can only sense the insignificant and low-frequency (< 25Hz) sounds caused by muscle friction; therefore, applying the technology outside the laboratory needs trained personnel. AMG has been reported to be superior to surface EMG for estimating the ESTi® score.[10] AMG is reported to be effective for measuring prestress under the effects of anisotropy and acoustoelastography.[20]

Different from measuring the mechanical properties of muscular fibers using ultrasound, popular technologies measure or evaluate the functionality of a group of muscles through the vibration of muscle or electricity, for example, MMG, phonomyography, acceleromyography (VMG),[21], and EMG.[22–26] VMG estimates the muscle condition on the basis of attached points' balance, motion, and bending. EMG measures the electric pulse leaked to the surface of the skin. Because EMG signals have low intensity and are mixed with other bioactivities, experiments often need to be conducted in a well-shielded laboratory to reject environmental electronic noise; therefore, clinical applications are limited.[10] MMG's extremely low frequency vibration makes it difficult to measure moving objects, and the MMG device is generally applied to isometric muscle contraction.[27–29]

Deep generative modeling has been prevalently used recently. Generative adversarial networks (GANs) consist of two competing models in the training process, a min-max two-player game.[30] Various extensions of GANs have reported excellent results in a wide range of applications.[31–33] The boosting and bagging algorithm has been reported to have excellent capability in resisting noisy and imbalanced data.[34,35] This algorithm can effectively separate

good samples from bad ones when a sufficient set of features is applied.[36] Ensemble empirical mode decomposition and correlation dimension have also been reported to enhance the classification performance.[37,38] Ensemble learning, which takes advantage of various machine learning models, is also reported to be adequate for difficult modeling situations.[38–40]

2. Materials and Methods

2.1 Problem definition

The SIRM device produces synthetic audible sounds and injects them into the inspecting muscle through an impedance coupler. The sounds traverse through the medium and are then received by the contact microphone at the other end of the muscle. The injected sounds change the composition of the spectrum as the muscle contracts, and then the internal shear modulus is estimated.

The proposed SIRM is built on the basis of the characteristics of a modified myophonogram. AMG and MMG are combined to emit sound waves into tissues, which are then analyzed through the other end of the tissues. The critical part of the approach involves data generation and model learning. Previous approaches are insufficient in recognizing the difference in sound response between different muscle contents.

In Fig. 1, the proposed intelligence model works in two phases: model training and model usage. At the model usage phase, with the resulting three digital twins (*DT*s), we take the sound response from a muscle (*in vivo*) and predict the performance index (*PI*) of such a muscle. The sound samples are standardized to a single response/excitation (*RE*) signal through a pair of input/output spectra. The model DT_m maps the $RE = \{RE_i\}_{i=1,2,3}$ to a set of physical parameters ($P = \{P_i\}_{i=1,2,3}$), whereas the model DT_t maps the signals to a set of transformed features ($T = \{T_i\}_{i=1,2,3}$). Finally, the model DT_f maps the extracted vectors into a muscle *PI*.

Before the model can be used, a training phase must be taken offline. To train the DT models, we must collect the data representing the complete relation of input and output. Unfortunately, some input data may not be easily obtained. For example, one of the muscle's intrinsic parameters, such as Young's modulus, may not be measured easily. We set the data tuples $X_1 = (T_1, P_1)$, $X_2 = (T_2, P_2)$, $X_3 = (T_3, P_3)$. An artificially made phantom can solve part of the problem; therefore, we can collect a primary set of input/output data pairs (RE_1, X_1). However, the phantom may not cover all the properties of an actual muscle. We need to resort to other ways to generate the data.

In this study, we used the partial differential-equation-based simulation to generate sound responses (*in vitro*) according to a list of permutations from all possible parameter combinations. Note that this generation type is not equivalent to the simulation concept. The simulation is performed by fixing a predetermined set of parameters. Our *in vitro* generation enumerates all possible combinations of parameter pairs (RE_2, X_2) and thus covers a large variety of phantoms.

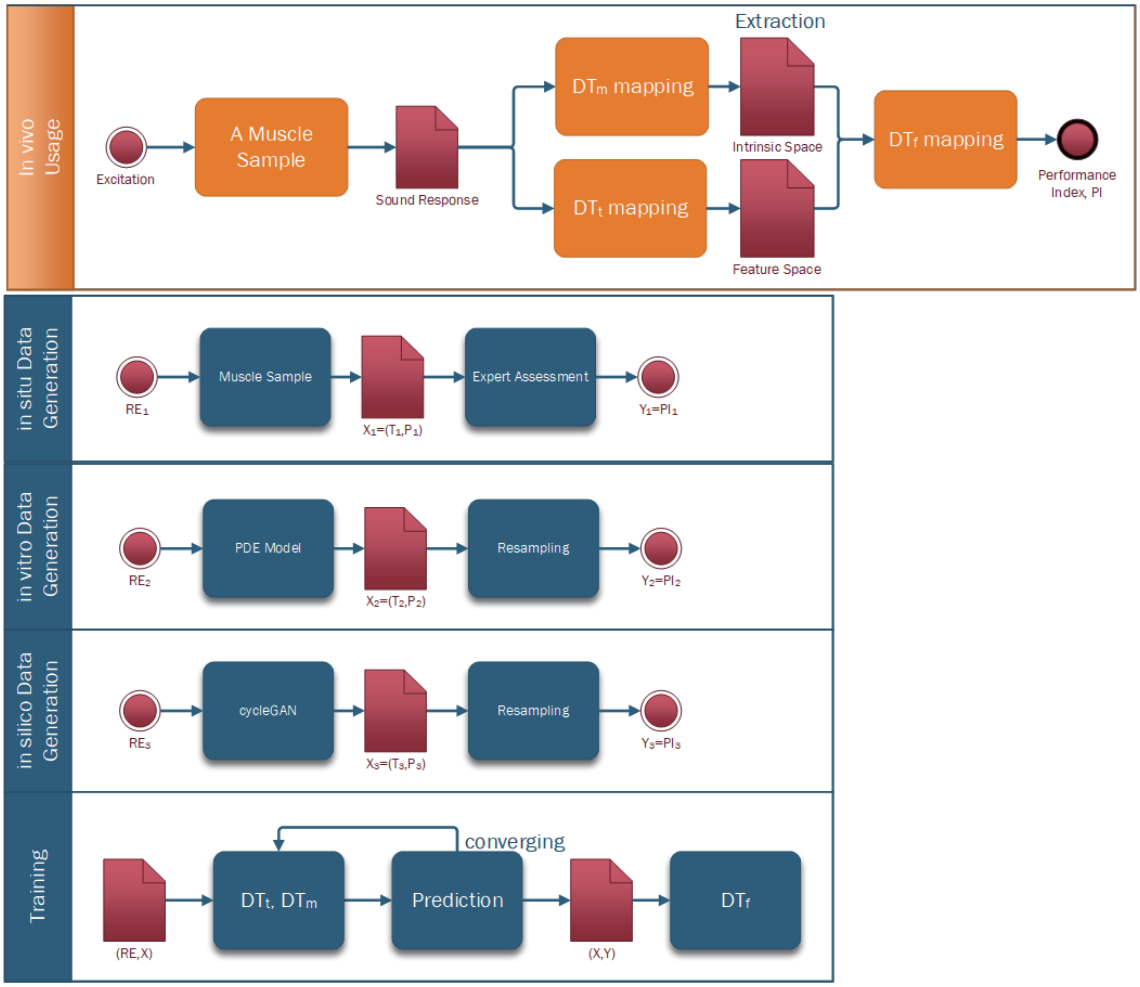

Fig. 1. (Color online) Before SIRM can be used, three *DT*s must be trained on the basis of the collected data. The model usage is in vivo. Given a living muscle, we inject a pattern of sounds and receive a sound response. We standardize the input/output spectrum pair to a single *RE* signal. The model DT_m maps the RE to a set of physical parameters (P), while the model DT_t maps the signals to a set of transformed features (T). Finally, the model DT_f maps the extracted vectors into a muscle *PI*. DT_t is pre-designed in a set of transformations, such as the entropy value of the Fourier transform. Therefore, DT_t does not need to be trained from data. To train DT_m, we need to collect a pair of input (*RE*) and output (P) data. Because the muscle properties are mostly unmeasurable, the data generation processes are performed *in situ*, *in vitro*, and *in silico*. In the *in situ* case, we take actual samples to measure the sound response. In the *in vitro* case, the sound responses are generated by mathematical models. In the *in silico* case, the sound responses are generated by the cycle-GAN model.

On the other hand, we may not consider all situations in the phantoms. We also generated a large set of random data by altering the data in the latent space. The input/output data pair (RE_3, X_3) was generated in an *in silico* step through the cycle-GAN model.[41]

As shown in the bottom block of Fig. 1, once the data sets ($RE = \{RE_i\}_{i=1,2,3}$, $X = \{X_i\}_{i=1,2,3}$) and ($X = \{X_i\}_{i=1,2,3}$, $Y = \{Y_i\}_{i=1,2,3}$) are prepared, DT_t, DT_m, and DT_f can be trained through our inverse mapping algorithms.

2.2 Muscle data preparation for DT_m using shear modulus and stiffness

Propagating sounds in a medium (soft tissue) can be modeled scientifically. The governing equations in the conservation equations and pressure–density relation for the nonlinear propagation of acoustic waves have been extensively studied.[42] The equations in a heterogeneous and moving turbulent fluid can be modeled.[43] Let $\boldsymbol{u}$ be the acoustic particle velocity, p the acoustic pressure, ρ the acoustic density, ρ_0 the ambient (or equilibrium) density, and c_0 the isentropic sound speed. First, we look at a base model in the propagating medium that is quiescent (no net flow and time-invariant ambient parameters), isotropic, and inviscid (no viscosity).

For the quiescent, isotropic, and inviscid heterogeneous medium, the nonlinear propagation of compressible acoustic waves can be expressed as

$$\dot{\boldsymbol{u}} + \nabla p = -\rho\dot{\boldsymbol{u}} - \frac{1}{2}\rho_0 \nabla\left(u^2\right), \tag{1}$$

$$\dot{\rho} + \nabla \cdot \left(\rho_0 \boldsymbol{u}\right) = -\nabla \cdot \left(\rho \boldsymbol{u}\right), \tag{2}$$

$$p = c_0^2 \rho, \tag{3}$$

where $u^2 = \boldsymbol{u} \cdot \boldsymbol{u}$.

Sound absorption follows a power law in the spectrum distribution, which assumes an anisotropic perfectly matched layer in the absorption of acoustic waves. When the acoustic waves exceed a certain amplitude, the wave propagation becomes nonlinear, and, therefore, tissues should be assumed heterogeneous. The heterogeneous Westervelt equation in Lagrangian coordinates is considered.[44] The absorption mechanisms in soft tissues, such as vibrational, structural, and chemical relaxations, can be complex, and, therefore, the observed attenuation $\alpha = \alpha_0 \omega^y$ can be modeled to an absorption coefficient, *1*, where α_0, y, and ω are the power law prefactor, exponent, and wave frequency, respectively, in the range of 1–1.5.[45,46]

In soft tissues, a shear wave induces particle movement perpendicular to the direction of the wave propagation with shear speed (c_s), typically ranging between 1 and 10 m/s.[47] Unlike longitudinal waves, the propagation of the shear wave does not change the local density of the medium. For a purely elastic and isotropic medium, c_s is directly related to the shear modulus. In incompressible media or biological tissues, we also know that μ is approximately one-third of Young's modulus, which is the ratio of the longitudinal stress to the longitudinal strain, and represents the tendency of the medium to deform axially when forces opposite and parallel to this axis are applied.[48]

Most GAN applications use neural networks entirely for classification and regression applications. In our application, we hybridize a statistical generator and a neural network discriminator to maximize the use of prior model information for the stochastic process. Our generator has the advantage given that it takes environmental conditions as covariates in the

random process and is robust to an anti-symmetric station distribution. A standard GAN consists of a generator G and a discriminator D.[30] The G and D models can be neural networks or any mathematical functions, as long as Eq. (4) has a solution. For any observed data pairs (x, y) and latent vector s,

$$G^* = \arg\min_G \max_D L_{GAN}(G,D) + \lambda L_{l_1}(G), \tag{4}$$

where λ is the perturbation coefficient and the loss functions $L_{GAN}(G, D) = E_{x,y}[\log D(x, y)] + E_{x,s}[\log(1 - D(x, G(x, s)))]$ and $L_{l_1}(\mathrm{G}) = E_{x,y,s}[|y - G(x,s)|_1]$ with expectation E in l_1.

The discriminator is directly formed by the model's regular residual neural network. The network adds some jump connections that skip internal layers to avoid the vanishing gradient and accuracy saturation problems.[49] The network construction repeats a fixed pattern several times in which the strided convolution downsampler jumps, bypassing every two convolutions.

2.3 DT_t development in acoustic feature space

We developed DT_t in acoustic feature space through a set of transformations. The properties of muscles and each tissue medium are different, and the related properties, such as the vibration attenuation coefficients, are different for individual frequencies. The transfer function of the tissue medium can be obtained by injecting a theoretical impulse or homogeneous Gaussian white noise. When a Gaussian white noise is fed, a sound wave spectrum related to density and elasticity can be obtained at the other end.

However, because a muscle is not a complete fluid, the absorption attenuation superimposed by different amplitudes is nonlinear. Therefore, the amplitude is strengthened by the injected sound wave spectrum and also by the frequency bands with high attenuation. On the other hand, when muscles are undergoing isoaxial contraction, changes in density and elasticity also change the decay coefficient at each frequency band.

Theoretically, a particular spectrum for estimating the transfer function may be generated. However, because the energy injected by the sound generator is limited, the received spectrum may change nonlinearly. We use machine learning to solve this problem.

To extract useful features of the acoustic response signals for effective processing, many estimation methods have been developed, from traditional ones, such as the power spectrum from Fourier transforms, to advanced ones, such as the instantaneous frequency (*IF*) for nonstationary quasi-periodic signals. The *IF* can be obtained by performing wavelet ridge analysis such that $IF = \max_{a,t} \Re\{\ln |W_\phi(a, t)|\}$ and on the a-axis and $\max_t \frac{\partial}{\partial t} \Im\{\ln |W_\phi(a, t)|\} = \omega_\phi/a$ for the wavelet transform $W_\phi(a, t)$ of a time series.

2.4 Training of DT_m and DT_f

In the training of DT_f, we delegated the muscle *PI* to the absolute maximum muscle strength (kgw) when the quadriceps performs maximum voluntary contraction. We propose a training

algorithm, SEA, to associate the feature and parameter spaces [$X = (T, P)$] to the PI ($Y = PI$). The algorithm takes the functionals and l_1 space optimization by avoiding interference without overfitting. The challenge for individual learners in DT_f encountered in the mapping problem is to avoid overfitting. The learning task is a process of optimization, i.e., evaluating solutions in the l_1 norm space for DT_f, and thus, overfitting can be reduced.

Although the elastic modulus of muscle fibers is already a physical feature, it is still not the whole dimension compared with comprehensive muscle performance, and for an average individual, it cannot correspond to the training intensity and effect.

3. Results and Discussion

In the human body's muscle tests, the intrinsic parameters of muscles were estimated through our nondestructive muscle measurements, as shown in Fig. 2. Using the injected sound waves, we measured the physical characteristics of muscles nondestructively.

The sound spectrum and recording experiments were conducted under known conditions to capture the relationship between the injection spectrum and tissue absorption in motion accurately. We first conducted laboratory experiments on normal muscle tissues. A sample plan was also carried out to test the density of the triceps muscles on the core of the upper arm. We recruited five subjects with various body shapes, and the experiments consisted of resting (#2, #4, and #6) and motion sampling (#8, #10), measuring the muscles at the same locations for different directions, intensities, and fatigue states, and obtaining several muscle evaluation

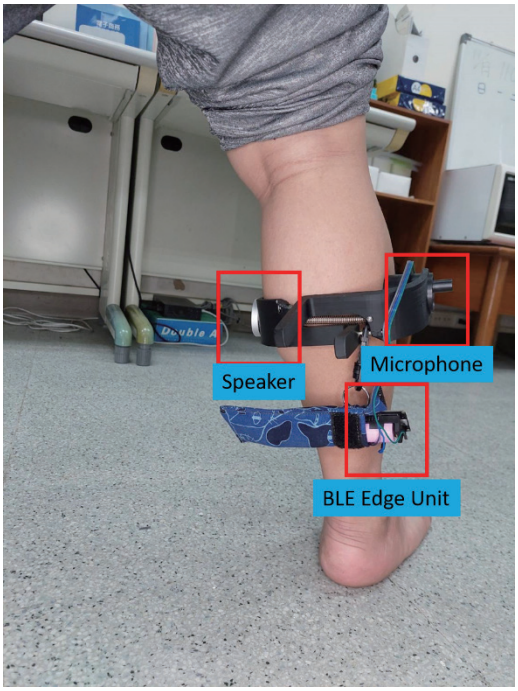

Fig. 2. (Color online) Our SIRM prototype transmits the raw recordings back to the computer hosting DTs through a Bluetooth edge unit.

indexes by experts and instruments. The muscle assessment of the *PI* is made in five levels of the ordinal scale, which can be converted to the quantity scale easily for our mapping algorithm.

Like MMG, contact microphones are sensitive to friction sound on the skin's surface during the test. However, our tolerance to friction is high because our generated sound can produce high-signal-to-noise ratio (SNR) signals in a short time. The recording experiments for each muscle sample are conducted over three months, and each sampling is repeated at least 10 times for a 30 s duration.

As shown in Fig. 3, we injected a wide range of sound waves into the muscle to counteract the nonlinear distortion caused by the soft tissue. After conduction, the resulting absorption spectrum was based on the mathematical model, and then the tissue structure of the target muscle was inferred in reverse order. Sound waves in Fig. 3 are designed to penetrate fat or water and produce versatile response results after traversing the muscle fibers, which can be used to analyze the distribution of muscle and fat in the body. A total of 50 audio samples, each 12 s in length, were obtained. After segmenting to 1 s frames, we obtained a total of 550

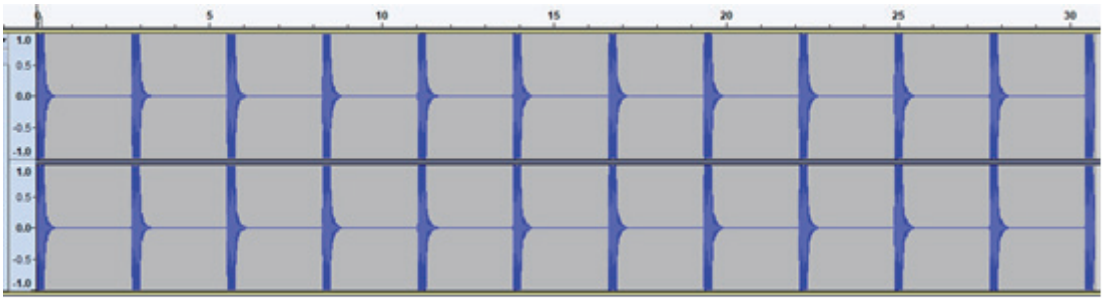

(a)

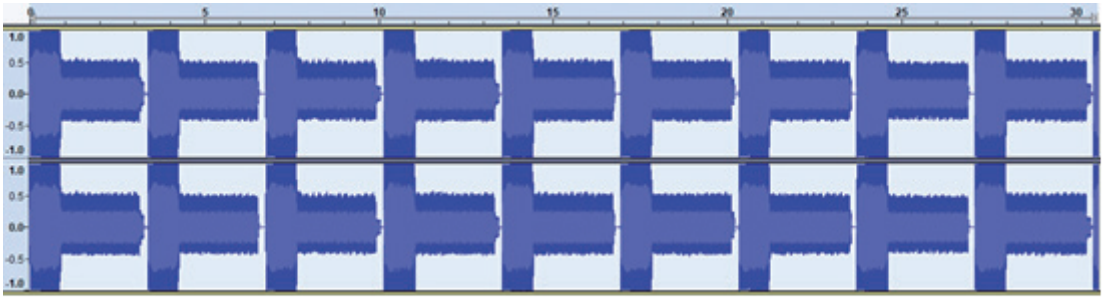

(b)

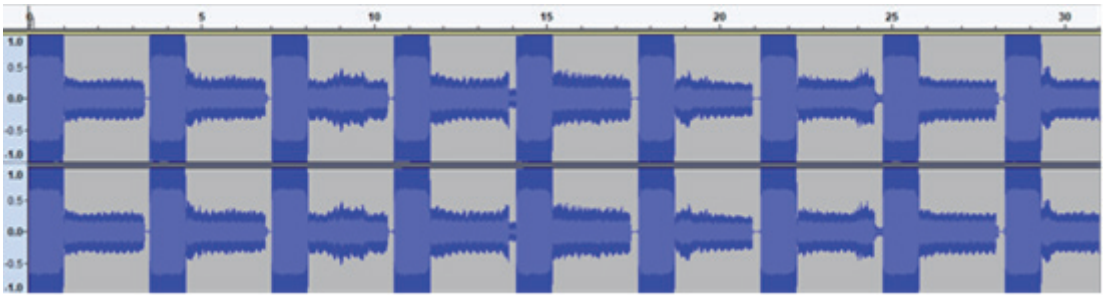

(c)

Fig. 3. (Color online) Three samples of injected sounds: (a) burst, (b) trumpet, and (c) drum chirps.

Table 1
Hit counts and confusion matrix for the testing set.

	Level-1	Level-2	Level-3	Level-4	Level-5
Level-1	13	0	2	0	0
Level-2	1	23	0	0	0
Level-3	1	0	22	0	0
Level-4	0	0	0	19	4
Level-5	0	0	0	0	25
Accuracy = 92.72%					

analyzable frames. We randomly chose 80% as the training set and 20% as the testing set. Therefore, 440 and 110 frames were used in the training and testing sets, respectively.

By the proposed method, we trained the cycle-GAN model to fine-tune the correct value of the muscle parameters. As a basis for data assimilation in muscle identification, we demonstrated our ability to estimate parameters. Our estimation can restore the internal parameters on the basis of the highest Bayesian probability.[50] The simulation data is twofold. Although limited observation data is available in muscle samples, we can synthesize them through the cycle-GAN model in a tissue medium. The collected sound converges with the data assimilation technique to estimate the internal modulus coefficient of the medium. The model and parameters were calibrated to match the simulation and measurement.

With training data, features were generated using DT_{m} and DT_t. DT_f was used for prediction based on the transformed feature. Because our scale of muscle *PI* is ordinal, the mapping result can be ordered in a category to count the hit rate. We also obtained the hit rate by comparing the training and testing samples.

Through the assimilation process in SIRM, DT only takes 0.5 s, and the testing accuracies are as shown in the confusion matrix in Table 1. Although the outputs of the final DT_f are continuous numbers, we arranged them into categories for easy representation of the confusion matrix. We obtained a comparative result of 92.7%.

4. Conclusions

Our SIRM is a low-cost, portable, and nondestructive muscle cross-section measurement device with no attached electrodes. Using the SEA technology, we used the injected and received sound waves to develop the muscle strength index. The results of this study are expected to contribute significantly to academic research, industry, national development, and other applications. This research can help the elderly or muscle-deficient patients carry out specific training and balance the cell destruction due to training overload and tissue reconstruction during body repair.

For an individual patient, knowing overtraining or undertraining is essential. A low-cost and convenient device can be placed on the body anytime without affecting the movement. To prevent overtraining, the device can advise whether the training can proceed or be stopped. Therefore, the probability of injury can be significantly reduced under the premise of the training device. By recording the training journey for muscle development, a patient can

understand their muscle condition ahead of time. For the physician, through the SIRM, the entire training process can be adequately moderated and can help accumulate experience for future planning. We can make the training programs effective by relying on real-time feedback information.

Acknowledgments

This work was supported in part by the National Science and Technology Council, Taiwan, under Grant nos. NSTC 112-2221-E-037-004-MY3, NSTC 112-2218-E-992-004, MOST 110-2622-E-992-026, and NSTC 112-2221-E-153-004. The authors also thank Yuan's General Hospital (Grant no. ST110005), NKUST-KMU joint research project (Grant no. NKUSTKMU-112-KK-009), and NSYSU-KMU joint research project (Grant no. NSYSU-KMU-113-P07).

References

1 Z. A. Puthucheary, R. Phadke, J. Rawal, M. J. W. McPhail, P. S Sidhu, A. Rowlerson, J. Moxham, S. Harridge, N. Hart, and H. E. Montgomery: Crit. Care Med. **43** (2015) 1603. https://doi.org/10.1097/CCM.0000000000001016
2 M. Krix, M.-A. Weber, K.-R. Holger, H. B. Huttner, S. Delorme, H.-U. Kauczor, and W. Hildebrandt: J. Ultrasound Med. **24** (2005) 431. https://doi.org/10.7863/jum.2005.24.4.431
3 J. Siracusa, K. Charlot, A. Malgoyre, S. Conort, P.-E. Tardo-Dino, C. Bourrilhon, and S. Garcia-Vicencio: Front. Physiol. **10** (2019) 626. https://doi.org/10.3389/fphys.2019.00626
4 B. T. H. M. Sleutjes, C. A. Wijngaarde, R. I. Wadman, L. A. M. Otto, F.-L. Asselman, I. Cuppen, L. H. van den Berg, W. L. van der Pol, and H. S. Goedee: Clin. Neurophysiol. **131** (2020) 1280. https://doi.org/10.1016/j.clinph.2020.01.018
5 A. Islam, K. Sundaraj, B. Ahmad, N. U. Ahamed, and A. Ali: J. Phys. Ther. Sci. **24** (2012) 1359. https://doi.org/10.1589/jpts.24.1359
6 E. M. Bartels, J. K. Olsen, E. L. Andersen, B. Danneskiold-Samsøe, H. Bliddal, L. E. Kristensen, and A. P. Harrison: Curr. Res. Physiol. **2** (2020) 22. https://doi.org/10.1016/j.crphys.2020.02.002
7 A. Buis, F. Guarato, J. Law, Z. Ralston, and A. Courtney: Can. Prosthet. Orthot. J. **1** (2018) 1. https://doi.org/10.33137/CPOJ.V1I1.30354
8 G.-X. Xu, P.-Y. Chen, X. Jiang, and C.-C. Huang: IEEE Trans. Biomed. Eng. **69** (2022) 2745. https://doi.org/10.1109/TBME.2022.3152896
9 MyoDynamik: ESTi score, 2024. https://myographytech.com (accessed March 2024).
10 A. P. Harrison: Clin. Physiol. Funct. Imaging **38** (2018) 312. https://doi.org/10.1111/cpf.12417
11 A. P. Harrison, D.-S. Bente, and E. M. Bartels: Physiol. Rep. **1** (2013) e00029. https://doi.org/10.1002/phy2.29
12 N. Miyamoto, K. Hirata, H. Kanehisa, and Y. Yoshitake: PLOS ONE **10** (2015) e0124311 https://doi.org/https://doi.org/10.1371/journal.pone.0124311
13 K. M. M. E. Lima, J. F. S. Costa Júnior, W. C. de A. Pereira, and L. F. De Oliveira: Ultrasonography **37** (2018) 3. https://doi.org/10.14366/usg.17017
14 I. Imura, Y. Gotoh, K. Sakai, Y. Ohara, J. Tazoe, H. Miura, T. Hirota, A. Uchiyama, and Y. Nomura: Sens. Mater. **34** (2022) 2955. https://doi.org/10.18494/sam3908
15 M. A. James: J. Hand Surg. **32** (2007) 154. https://doi.org/10.1016/j.jhsa.2006.11.008
16 P.-S. Tatjana, G.-S. Martina, P. Martin, S. Othmar, V. Gerda, M. Christian, B. Christian, and F.-M. Veronika: J. Rehabil. Med. **40** (2008) 665. https://doi.org/10.2340/16501977-0235
17 T. D. Roza, T. Mascarenhas, M. Araujo, V. Trindade, and R. N. Jorge: Physiotherapy **99** (2013) 207. https://doi.org/10.1016/j.physio.2012.05.014
18 W.-A. Lai, S.-H. Lin, Y.-T. Wang, and Y.-C. Wang: Sens. Mater. **34** (2022) 1943. https://doi.org/https://doi.org/10.18494/SAM3594
19 C.-M. Shih, J. M. Lai, Y.-K. Chan, M. Y. Hsieh, and T.-H. Meen: Sens. Mater. **35** (2023) 2771. https://doi.org/10.18494/SAM4456
20 J. Crutison, M. Sun, and T. J. Royston: J. Acoust. Soc. Am. **151** (2022) 2403. https://doi.org/10.1121/10.0010110

21 T. W. Beck, T. J. Housh, G. O. Johnson, J. T. Cramer, J. P. Weir, J. W. Coburn, and M. H. Malek: J. Electromyogr. Kines. **17** (2007) 1. https://doi.org/10.1016/j.jelekin.2005.12.002
22 M. Bernardi, F. Felici, M. Marchetti, F. Montellanico, M. F. Piacentini, and M. Solomonow: J. Electromyogr. Kines. **9** (1999) 121. https://doi.org/10.1016/j.jelekin.2005.12.00210.1016/S1050-6411(98)00043-1
23 S. Karlsson and B. Gerdle: J. Electromyogr. Kines. **11** (2001) 131. https://doi.org/10.1016/s1050-6411(00)00046-8
24 B. Larsson, F. Kadi, B. Lindvall, and B. Gerdle: J. Electromyogr. Kines. **16** (2006) 281. https://doi.org/10.1016/j.jelekin.2005.07.009
25 Q.-H. Huang, Y.-P. Zheng, C. X, J. F. He, and J. Shi: Open Biomed. Eng. J. **1** (2007) 77. https://doi.org/10.2174/1874120700701010077
26 J. Shi, Y.-P. Zheng, Q.-Hua Huang, and X. Chen: IEEE Trans. Biomed. Eng. **55** (2008) 1191. https://doi.org/10.1109/TBME.2007.909538
27 M. Watakabe, Y. Itoh, K. Mita, and K. Akataki: Med. Biol. Eng. Comput. **36** (1998) 557. https://doi.org/10.1007/BF02524423
28 M. Watakabe, K. Mita, K. Akataki, and K. Ito: Med. Biol. Eng. Comput. **41** (2003) 198. https://doi.org/10.1007/BF02344888
29 M. Watakabe, K, Mita, K. Akataki, and Y. Ito: Med. Biol. Eng. Comput. **39** (2001) 195. https://doi.org/10.1007/BF02344804
30 I. Goodfellow, P.-A. Jean, M. Mirza, B. Xu, W.-F. David, S. Ozair, A. Courville, and Y. Bengio: Advances Neural Information Processing Systems (NIPS, 2014) 2672.
31 L. Tian, X. Li, Y. Ye, P. Xie, and Y. Li: IEEE Geosci. Remote Sens. Lett. **17** (2019) 601. https://doi.org/10.1109/LGRS.2019.2926776
32 C. Chaudhuri and C. Robertson: Water **12** (2020) 3353. https://doi.org/10.3390/w12123353
33 Y. J. Chen, J.-T. Tsai, C.-L. Chen, and W.-H. Ho: AIMS Math. **8** (2023) 27989. https://doi.org/10.3934/math.20231432
34 T. M. Khoshgoftaar, J. V. Hulse, and A. Napolitano: IEEE Trans. Systems, Man, and Cybern. Part A Syst. Humans **41** (2011) 552. https://doi.org/10.1109/TSMCA.2010.2084081
35 Y. J. Chen, Y.-C. Liou, W.-H. Ho, J.-T. Tsai, and C.-C. Liu: Sci. Prog. **104** (2022) 1. https://doi.org/doi.org/10.1177/003685042211108
36 P. Das and K. Chanda: Climate Change and Water Security (Springer, 2022) 117. https://doi.org/10.1007/978-981-16-5501-2_10
37 W. Zhang, X. Guo, Z. Yuan, and X. Zhu: J. Mech. Med. Biol. **14** (2014) 1450046. https://doi.org/10.1142/S0219519414500468
38 W.-H. Ho, C.-T. Liao, Y. J. Chen, K.-S. Hwang, and Y. Tao: IEEE Access **10** (2022) 51079. https://doi.org/10.1109/ACCESS.2022.3173176
39 J. M Drake, C. Randin, and A. Guisan: J. Appl. Ecol. **43** (2006) 424. https://doi.org/10.1111/j.1365-2664.2006.01141.x
40 C. Wu, M. Hwang, T.-H. Huang, Y. J. Chen, Y.-J. Chang, T.-H. Ho, J. Huang, K.-S. Hwang, and W.-H. Ho: BMC Bioinf. **22** (2021) 1. https://doi.org/10.1186/s12859-021-04000-2
41 B.-H. Su and C.-C. Lee: IEEE Trans. Affect. Comput. **14** (2023) 1991. https://doi.org/10.1109/TAFFC.2022.3146325
42 M. F Hamilton, D. T. Blackstock: Nonlinear Acoustics (Academic Press, San Diego, 1998).
43 F. Coulouvrat: Wave Motion **49** (2012) 50. https://doi.org/10.1016/j.wavemoti.2011.07.002
44 G. Taraldsen: J. Acoust. Soc. Am. **109** (2001) 1329. https://doi.org/10.1121/1.1344157
45 M. J. Buckingham: J. Acoust. Soc. Am. **102** (1997) 2579. https://doi.org/10.1121/1.420313
46 J. C. Bamber: Attenuation and Absorption: Physical Principles of Medical Ultrasonics (John Wiley & Sons, 2004) pp. 93–166.
47 R. S. C. Cobbold: Foundations of Biomedical Ultrasound (Oxford University Press, 2006) p. 802.
48 D. Royer and E. Dieulesaint: Elastic Waves in Solids I: Free and Guided Propagation (Springer Science & Business Media, 1999) p. 374.
49 L. Yan, J. Feng, T. Hang, and Y. Zhu: Appl. Soft Comput. **104** (2021) 107228. https://doi.org/10.1016/j.asoc.2021.107228
50 C.-H. Lee, K. Chang, Y.-M. Chen, J.-T. Tsai, Y. J. Chen, and W.-H. Ho: BMC Bioinf. **22** (2021) 1. https://doi.org/10.1186/s12859-021-04059-x